Mon. Not. R. Astron. Soc. **316**, 129–136 (2000)

ASCA spectroscopy of the hard X-ray emission from the colliding wind interaction in γ^2 Velorum

G. Rauw,[1,2★†] I. R. Stevens,[2★] J. M. Pittard[2,3★] and M. F. Corcoran[4★]

[1]*Institut d'Astrophysique & Géophysique, Université de Liège, 5, Avenue de Cointe, B-4000 Liège, Belgium*
[2]*School of Physics & Astronomy, University of Birmingham, Edgbaston, Birmingham B15 2TT*
[3]*Department of Physics & Astronomy, University of Leeds, Woodhouse Lane, Leeds LS2 9JT*
[4]*USRA/LHEA, Goddard Space Flight Center, Greenbelt, MD 20771, USA*

Accepted 2000 February 16. Received 2000 January 31; in original form 1999 July 9

ABSTRACT

We discuss an *ASCA* observation of the eccentric WC8 + O7.5 III binary γ^2 Velorum near apastron. The X-ray spectrum is compared with two previous observations obtained when the system was near periastron. All three spectra display a hard-emission component that undergoes strong variability over the orbital cycle. The properties of the hard X-ray emission of γ^2 Vel are constrained by taking into account the contribution from contaminating soft X-ray sources in the vicinity of γ^2 Vel. We find that the observed variations are in qualitative agreement with the predictions of colliding wind models. We investigate for the first time the effect of uncertainties in the chemical composition of the X-ray emitting plasma on our understanding of the high-energy properties of the wind interaction region. Our results indicate that these uncertainties significantly affect the derived shock temperature and absorption column, but play a smaller role in determining the intrinsic X-ray luminosity of the colliding wind zone. We further find that the intrinsic luminosity from the hard X-ray component in γ^2 Vel does not follow the $1/D$ distance relation expected from simple models of adiabatic shocks.

Key words: binaries: general – stars: individual: γ^2 Vel – stars: mass-loss – stars: Wolf–Rayet – X-rays: stars.

1 INTRODUCTION

The eccentric Wolf–Rayet binary γ^2 Velorum (=HD 68273 =WR 11, $P_{\rm orb} = 78.53$ d, $e = 0.326$) is a cornerstone for our understanding of many fundamental aspects of the Wolf–Rayet phenomenon and of massive stars in general, and has therefore been studied extensively at many different wavelengths.

Recently, the distance of γ^2 Vel was determined from *Hipparcos* parallax measurements to be 258^{+41}_{-31} pc (Schaerer, Schmutz & Grenon 1997; van der Hucht et al. 1997). Consequently, the former classification of the O-star component as a supergiant (Conti & Smith 1972) had to be revised and γ^2 Vel is now classified as WC8+O7.5 III (De Marco & Schmutz 1999). The revised distance also leads to a smaller radio mass-loss rate of $\dot{M} = (2.8 \pm 1.0) \times 10^{-5}\,{\rm M}_\odot\,{\rm yr}^{-1}$ for the WC8 star (Leitherer, Chapman & Koribalski 1997; Schaerer et al. 1997). In light of these results, the properties of the O-star component were investigated by De Marco & Schmutz (1999). From a hydrodynamic atmosphere/wind model, these authors derive a mass-loss rate of $\dot{M} = (1.8 \pm 0.4) \times 10^{-7}\,{\rm M}_\odot\,{\rm yr}^{-1}$ for the O-star.

Over the last two decades, observations of γ^2 Vel have provided strong evidence for an interaction between the winds of the WC8 star and its O-star companion. St.-Louis, Willis & Stevens (1993) have studied an extensive set of high-resolution *IUE* spectra of γ^2 Vel. These authors report strong phase-locked line profile variability that they describe as a result of the combination of selective atmospheric eclipses and the effect of a cavity in the WR wind produced by the wind collision.

Radio and millimetre observations of γ^2 Vel revealed essentially a thermal spectrum (Abbott et al. 1986; Williams et al. 1990b; Leitherer et al. 1997) with no clear indication of a non-thermal component arising in the shock region, contrary to what is observed in the very wide WC7+O4–5 binary WR 140 (Williams et al. 1990a). However, Chapman et al. (1999) found a steepening of the radio spectral index of γ^2 Vel between 3 and 20 cm. This could possibly indicate a highly attenuated non-thermal component originating deep within the wind.

Further support for a wind collision in γ^2 Vel comes from the *ROSAT* PSPC observations of this star gathered by Willis, Schild & Stevens (1995). These authors discovered substantial phase-locked variability of the X-ray flux from γ^2 Vel. The X-ray flux

★ E-mail: rauw@astro.ulg.ac.be (GR); irs@star.sr.bham.ac.uk (IRS); jmp@ast.leeds.ac.uk (JMP); corcoran@barnegat.gsfc.nasa.gov (MFC)
† Chargé de Recherches FNRS, Belgium.

strongly increases at orbital phases when the O-star passes in front of the WC8 component. Willis et al. (1995) attribute this increase to extra X-ray emission from a shock front between the two wind components. The X-ray emission from the shock is highly absorbed when the dense and opaque WR wind is in front. However, the colliding wind X-ray emission becomes significantly less absorbed at orbital phases when the cavity around the O-star crosses the line of sight. Stevens et al. (1996) discussed two *ASCA* observations of γ^2 Vel obtained at orbital phases when the O-star is in front of the WC8 component, and used a hydrodynamic model of colliding winds to calculate synthetic spectra that are then fitted to the *ASCA* spectra. They derive a mass-loss rate that is in reasonable agreement with the value derived from radio observations accounting for the revised distance determination (Schaerer et al. 1997).

In the present paper, we discuss an *ASCA* spectrum of γ^2 Vel obtained near apastron and we compare it with the two archival observations that were obtained near periastron. For the first time, we take into account the contamination by nearby point sources as derived from the *ROSAT* PSPC data of Willis et al. (1995). The data analysis is presented in Section 2. Different attempts to fit the spectra with thermal plasma models are discussed in Section 3, and our conclusions are given in Section 4.

2 *ASCA* OBSERVATIONS AND DATA REDUCTION

γ^2 Velorum has been observed with *ASCA* at three different orbital phases; two near-periastron exposures lasted over ~20 ks each, while the apastron observation covered about 30 ks. Throughout this paper we adopt the orbital phases with respect to periastron according to the ephemeris of Schmutz et al. (1997, hereafter S97):

$$\mathrm{JD(periastron)} = 245\,0120.00 + 78.53E$$

(see Table 1). To allow comparison with previous work (Willis et al. 1995; Stevens et al. 1996), Table 1 also provides the orbital phases according to the ephemeris of Moffat et al. (1986) with respect to conjunction (WR star in front).

For all three observations we retrieved the screened event files from the ARNIE data base at Leicester University, and we combined the high bit-rate and medium bit-rate data in our analysis. The raw light curves of these data were inspected and in one case (the apastron observation) we found on several occasions a sudden rise of the overall count rate shortly before the spacecraft entered the South Atlantic Anomaly. After testing different criteria to re-screen the data, it turned out that the most efficient way to remove these sudden background increases was to filter out the time intervals of low data quality. The remaining useful exposure times at $\phi = 0.570$ are 25 700 and 28 000 s for the SIS and GIS instruments, respectively.

Table 1. Journal of γ^2 Vel observations with the *ASCA* satellite.

Date JD-244 0000	ϕ (S97)	PA	ϕ' (M86)	Total elapsed phase interval
9 490.213	0.978	−38°	0.404	0.013
9 497.890	0.078	32°	0.502	0.008
10 164.773	0.570	172°	0.997	0.012

For each observation, we list the JD at mid-exposure and the corresponding orbital phase (with respect to periastron) and the mean position angle (with respect to the line of sight) according to the ephemeris of S97. A PA of 0° corresponds to the O-star being in front of the WR component. To make comparison with previous work easier, the fourth column provides the phase with respect to the conjunction (WR star in front) according to the ephemeris of Moffat et al. (1986). The last column lists the total phase interval elapsed between the start and stop times of the *ASCA* exposure.

The data reduction was performed with the XSELECT software (version 1.4b).

2.1 SIS spectra

For the two near-periastron observations, the source spectra were extracted from a circular region of 4-arcmin radius on the SIS0 detector. Since the source image is located slightly closer to the edge of chip 3 in the SIS1 frame, the extraction radius was reduced to 3.2 arcmin.

During the apastron observation, the source was located closer to the edge of the chip of the SIS0 and SIS1 detectors. The extraction radius was therefore limited to 3 and 2.2 arcmin, respectively. Consequently, up to about 15 per cent of the flux in the wings of the point spread function (PSF) could be lost for the SIS1 apastron spectrum.

We tested several methods of background subtraction:

(i) using the background from the whole chip outside the source region;

(ii) using a circular region on the chip, free from any (obvious) source contamination;

(iii) using archive blank-sky observations and extracting the background in the same circular region as the source.

Background subtraction methods (i) and (ii) provide nearly identical background corrections. A fit with a two-temperature Raymond–Smith-type plasma model (Raymond & Smith 1977) yielded overlapping fit parameters for both background-corrected spectra. Since the extraction region used in method (i) is larger than in method (ii), the number of background counts is larger and the statistical errors of the background spectrum derived by method (i) are slightly lower. In the following analysis of the SIS data we use the background spectra obtained by method (i).

2.2 GIS spectra

For the two near-periastron observations, the GIS2 source spectrum was extracted from a circular region of 6-arcmin radius. For the GIS3 data, a slightly smaller radius of 5.25 arcmin was used in order to avoid overlap of the source region with the background region, which was chosen to be diametrically opposite on the GIS detector.

During the apastron observation, the source was located slightly closer to the centre of the GIS field of view. We used extraction radii of 5 and 4.5 arcmin for the GIS2 and GIS3 data, respectively.

Two methods of background subtraction have been tested:

(i) using a circular region that is diametrically opposite to the source region (i.e. the background region has the same radius and same off-axis angle as the source region);

(ii) adding up archive blank-sky observations of different cut-off rigidity; the background spectrum is then extracted from the same circular region as the source but on the resulting blank-sky image.

The two background methods yield results that overlap within the

errors of the two-temperature fits. In the following we focus on the results obtained with the first background subtraction method.

2.3 Contaminating sources

The *ROSAT* PSPC observations of the γ^2 Vel field presented by Willis et al. (1995) reveal eight X-ray point sources within a radius of 4 arcmin around γ Vel. These sources are not resolved with *ASCA* and therefore contribute to the spectra extracted from the *ASCA* observations. As discussed by Stevens et al. (1996), there is very little information available on the nature of most of the contaminating sources. Two of them are known to be B-type stars and one is classified as a foreground Am star (Abt et al. 1976). However, no classification is known for the other sources.

Comparison between a SIS0 image in a hard energy band (2.0–6.0 keV) and in a soft energy band (0.5–2.0 keV) indicates that the harder emission is slightly more concentrated near the position of γ^2 Vel than the soft emission. This result suggests that, at all three orbital phases, γ^2 Vel is the main hard X-ray source in the field of view, whereas the nearby sources contribute a significant fraction of the soft emission. For instance, depending on the phase-dependent count rate of γ^2 Vel, the surrounding sources provide between 35 and 78 per cent of the total *ROSAT* PSPC count rate from a 4-arcmin radius region centred on γ^2 Vel.

In order to quantify this contamination, we retrieved the relevant *ROSAT* data from the ARNIE archive. We combined all the PSPC event lists and built the mean spectrum of the contaminating sources from two annular regions centred on γ^2 Vel with an inner radius of 1 arcmin and an outer radius of 3 or 4 arcmin, respectively. The PSPC background spectrum was extracted over four source-free circular regions of 10-arcmin radius each. The integrated PSPC count rate of the contaminating sources displays time variability by $\sim$10 per cent, i.e. at the 2σ level.

We fitted a two-temperature Raymond–Smith model to the mean PSPC spectrum of the sources around γ^2 Vel. The best-fitting parameters for extraction radii of 3 and 4 arcmin are listed in Table 2. We notice that these fits yield a column density towards the softer component that is only slightly larger than the interstellar column [$N_{\rm H}({\rm ISM}) = 8 \times 10^{19}\,{\rm cm}^{-2}$: Stevens et al. 1996] towards γ^2 Vel. A two-temperature plasma model with two distinct column densities was necessary to achieve a good fit to the PSPC spectrum of the contaminating sources. Adopting a single column density for both plasma components resulted in a poorer fit ($\chi^2_\nu = 1.48$ for model II), a column density close to $N_{\rm H}$(ISM) and a rather high kT_2 of 1.35 keV, much larger than the typical $kT \simeq 0.5$ keV of most B-type stars (e.g. Berghöfer, Schmitt & Cassinelli 1996).

Table 2. Best-fitting parameters of the mean PSPC spectrum of the contaminating sources. Models I and II correspond to an outer extraction radius of 3 and 4 arcmin, respectively. Within XSPEC, the emission measure EM is defined as $\int_V n_{\rm e} n_{\rm H}\,{\rm d}V$, where $n_{\rm e}$ and $n_{\rm H}$ are the electron and hydrogen densities, respectively. The emission measure corresponds to the *Hipparcos* distance of γ^2 Vel of 258 pc. The last row lists the integrated PSPC count rate of the contaminating source. For comparison the observed PSPC count rate of γ^2 Vel varies between 0.066 and 0.440 count s^{-1} depending on the orbital phase (see Willis et al. 1995).

Model	I	II
Outer extr. rad. (arcmin)	3	4
$(N_{\rm H})_1$ ($10^{22}\,{\rm cm}^{-2}$)	$(2.0^{+0.9}_{-0.6}) \times 10^{-2}$	$(1.7^{+0.7}_{-0.6}) \times 10^{-2}$
kT_1 (keV)	$0.16^{+0.04}_{-0.02}$	$0.17^{+0.04}_{-0.02}$
EM$_1$ ($10^{55}\,{\rm cm}^{-3}$)	3.52×10^{-2}	4.21×10^{-2}
$(N_{\rm H})_2$ ($10^{22}\,{\rm cm}^{-2}$)	$0.81^{+0.21}_{-0.25}$	$0.75^{+0.11}_{-0.25}$
kT_2 (keV)	$0.59^{+0.26}_{-0.25}$	$0.63^{+0.24}_{-0.15}$
EM$_2$ ($10^{55}\,{\rm cm}^{-3}$)	2.48×10^{-1}	2.58×10^{-1}
χ^2_ν (dof)	0.48 (14)	1.00 (14)
PSPC count rate (count s^{-1})	0.187	0.240

3 THE *ASCA* SPECTRUM OF γ^2 VEL

The SIS0 spectra of γ^2 Vel are displayed in Fig. 1. This figure illustrates the dramatic changes of the intensity and the spectral shape as a function of orbital phase. One also notices the prominent iron line at $\sim$6.7 keV, visible on all three spectra.

3.1 Spectral fitting

We modelled the extracted spectra using the XSPEC software (version 10.00). The spectra were rebinned to have at least 10 counts per bin and fitted with different models. It became immediately clear that a physically meaningful fit could only be achieved when the contaminating sources were taken into account. In fact, we tested various types of single-temperature and two-temperature Raymond–Smith and Mewe–Kaastra (Mewe, Gronenschild & van den Oord 1985; Kaastra 1992) models that did not take into account the effect of the nearby sources. Given the different sensitivities of the SIS and GIS instruments, we obtained quite different fit results for the SIS and GIS data sets. Part of these differences could actually reflect an instrumental effect leading to an increasing divergence of SIS and GIS spectra in the energy range below 1 keV (Hwang et al. 1999). Moreover, the physical interpretation of two-temperature fits in terms of X-ray emission from γ^2 Vel is rather difficult owing to the contamination by the nearby sources that is expected to affect mainly the softer component of the fits. In the following, we therefore include the effect of the contaminating sources in the spectral fits.

Assuming that the contaminating sources could be represented by the parameters listed in Table 2 at the time of the *ASCA* observations, we fitted the *ASCA* spectra with a three-temperature Raymond–Smith model keeping the parameters of two of the model components fixed at the values derived above (Table 2) for the contaminating sources. For this purpose, we used the spectral parameters of either the 3- or 4-arcmin (outer-radius) annulus depending on the actual radius used to extract the *ASCA* source spectrum (see Section 2). Only the parameters of the third component were varied in the fit, and the hard variable X-ray emission of γ^2 Vel was thus effectively fitted with a single-temperature Raymond–Smith model. Our fits reveal no trace of the very soft ($kT \simeq 0.19$ keV) emission component found by Willis et al. (1995) in the *ROSAT* PSPC spectra of γ^2 Vel. Because of the very different sensitivities of the *ROSAT* and *ASCA* instruments at energies below $\sim$1 keV, the *ROSAT* fit to the contaminating sources may slightly overestimate their actual contribution to the soft emission in the *ASCA* fits. Alternatively, it could be that the very soft component found by Willis et al. (1995) is itself variable and was weaker at the time of the *ASCA* observations.

The chemical composition of WC winds has been studied by means of ultraviolet (UV), optical and infrared (IR) spectroscopy revealing extremely non-solar abundances: H and N are totally

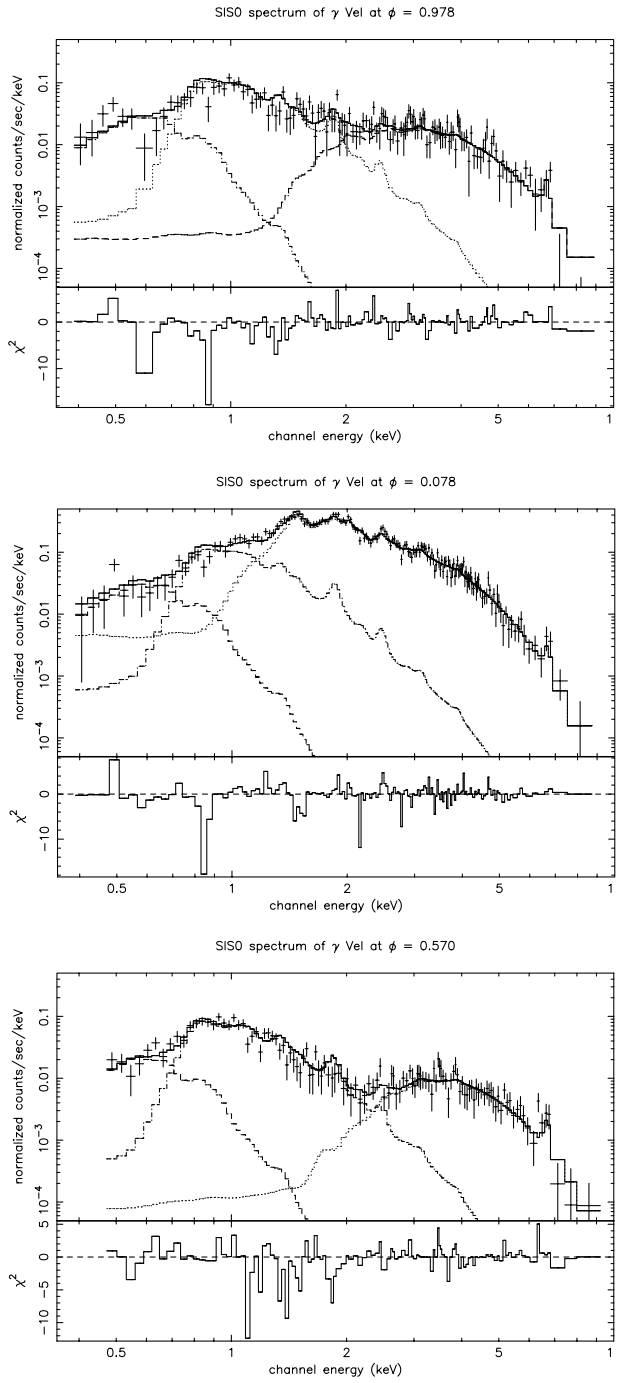

Figure 1. SIS0 spectra of γ^2 Vel at orbital phases $\phi = 0.978$ (top panel), 0.078 (middle panel) and 0.570 (bottom panel). The solid lines correspond to fits with a Raymond–Smith model including the effect of the contaminating sources and assuming a mixture between WC and O-star material of 50/50 by mass (see text). Note the prominent iron K line visible at all three orbital phases, whereas the other emission lines discussed in Section 3.2 are only visible on the $\phi = 0.078$ spectrum.

absent, whereas He, C and O are overabundant. From evolutionary considerations (e.g. Schaller et al. 1992), Ne, Mg and Si are also expected to be overabundant with respect to the solar abundances. Therefore, it seems natural to attempt an analysis of the *ASCA* spectra with non-solar abundance models.

There are, however, several limitations. Unfortunately, the

Table 3. Parameters of the hard component in the spectral fits of the SIS and GIS spectra of γ^2 Vel using a Raymond–Smith model accounting for the spectrum of the contaminating sources and assuming solar abundances. The label of the contaminating sources (I or II) refers to the two-temperature model parameters in Table 2. L_X and L_X^{int} are, respectively, the absorbed and intrinsic (i.e. absorption corrected) luminosities of the hard component in the energy range 0.5–10 keV. The emission measure and luminosities correspond to the *Hipparcos* distance of 258 pc.

Contam. sources	$\phi = 0.978$ II	$\phi = 0.078$ II	$\phi = 0.570$ I
varabs(0/100)*vray(0/100)			
N_H (10^{22} cm^{-2})	$7.5^{+0.9}_{-0.9}$	$2.40^{+0.06}_{-0.05}$	$11.9^{+1.7}_{-1.5}$
$\int \rho\, dz$ (10^{-2} g cm^{-2})	$17.82^{+2.12}_{-2.12}$	$5.72^{+0.14}_{-0.12}$	$28.36^{+4.05}_{-3.57}$
kT (keV)	$1.56^{+0.17}_{-0.12}$	$1.25^{+0.02}_{-0.02}$	$1.81^{+0.26}_{-0.23}$
EM (10^{55} cm^{-3})	1.85	6.16	1.43
χ^2_ν (dof)	1.14 (542)	1.35 (939)	1.28 (588)
L_X (10^{32} erg s^{-1})	0.27	1.51	0.20
L_X^{int} (10^{32} erg s^{-1})	2.49	9.01	1.92

ASCA data of γ^2 Vel are rather ill-suited to derive any constraints on the chemical abundances of the X-ray emitting plasma. The main reason is that the emission lines from the CNO elements are located in an energy region below 0.7 keV where the sensitivity of the instruments onboard *ASCA* is rather low and, moreover, the spectrum of γ^2 Vel in this energy range is seriously contaminated by the X-ray emission from the nearby soft sources. High-resolution spectroscopy with the *XMM* observatory might help to constrain the chemical abundances of the X-ray emitting plasma.

Another serious limitation comes from the fact that the colliding wind plasma, which is believed to produce the hard X-ray emission, consists of a mixture of WR and O-star wind material, with a priori unknown proportions. Although the pre-shock WC8 wind is denser, a greater fraction of the O-star wind is compressed and hence the O-star wind material affects the composition of the shocked plasma.

Moreover, the abundance anomalies of some key elements as predicted by the evolutionary models of WC stars depend critically on the ingredients (mixing, rotation, etc.) of these models (see, e.g., Meynet 1999). Thus any empirical model of the colliding wind plasma strongly depends on the assumed composition of the WC8 wind and the adopted mixture of the two winds. Similar remarks apply to the absorbing column towards the X-ray source, although in this case it seems likely that the absorption at phase $\phi = 0.570$ arises mostly from the WC8 wind material, whereas at phase $\phi = 0.078$ it probably arises from the sole O-star wind.

In view of these limitations, we opted for the following approach: we adopted average chemical abundances as listed by van der Hucht et al. (1986) except for the Ne abundance, which was taken from the recent results of Morris et al. (1999) derived from *ISO* SWS observations of γ^2 Vel. To simulate the chemical composition of the shocked plasma, we assumed a mixture between WC and O-star material of 0/100, 50/50 and 90/10 by mass, respectively. The photoelectric absorption was modelled using the cross-sections calculated by Bałucińska-Church & McCammon (1992) and adopting either the same abundances as for the emitting plasma or solar abundances.

Starting with the assumption that the bulk of the shocked gas comes from the O-star wind, we first used a 0/100 (i.e. solar abundance) model. In fact, it is possible that the majority of the X-ray emitting material might come from the shocked O-star wind

Table 4. As Table 3 except that we used non-solar abundances to model the composition of the emitting plasma and the absorbing column. The chemical composition of the shocked plasma was simulated assuming a mixture between WC- and O-star material of 50/50 and 90/10 by mass, respectively.

Contam. Sources	$\phi = 0.978$ II	$\phi = 0.078$ II	$\phi = 0.570$ I
varabs(50/50)*vray(50/50)			
$\int \rho \mathrm{d}z$ (10^{-2} g cm^{-2})	$1.40^{+0.19}_{-0.17}$	$0.46^{+0.01}_{-0.02}$	$2.17^{+0.27}_{-0.27}$
kT (keV)	$1.92^{+0.27}_{-0.23}$	$1.27^{+0.03}_{-0.03}$	$2.75^{+0.64}_{-0.39}$
EM (10^{55} cm^{-3})	0.20	0.91	0.12
χ^2_ν (dof)	1.14 (542)	1.46 (939)	1.30 (588)
L_X (10^{32} erg s^{-1})	0.27	1.49	0.20
$L_\mathrm{X}^\mathrm{int}$ (10^{32} erg s^{-1})	1.43	7.23	0.88
varabs(90/10)*vray(90/10)			
$\int \rho \mathrm{d}z$ (10^{-2} g cm^{-2})	$0.87^{+0.15}_{-0.09}$	$0.29^{+0.01}_{-0.01}$	$1.40^{+0.18}_{-0.17}$
kT (keV)	$1.97^{+0.23}_{-0.30}$	$1.27^{+0.03}_{-0.03}$	$2.74^{+0.67}_{-0.43}$
EM (10^{55} cm^{-3})	0.03	0.13	0.02
χ^2_ν (dof)	1.16 (542)	1.55 (939)	1.32 (588)
L_X (10^{32} erg s^{-1})	0.27	1.47	0.20
$L_\mathrm{X}^\mathrm{int}$ (10^{32} erg s^{-1})	1.34	7.00	0.87

Table 5. Best-fitting parameters of the most important emission lines in the $\phi = 0.078$ SIS and GIS spectrum of γ^2 Vel. Note that the equivalent widths are not corrected for the contribution of the serendipitous sources.

Ion	Line energy (keV)	Equiv. width (keV)
Mg XI	$1.45^{+0.02}_{-0.02}$	0.51
Si XIII	$1.89^{+0.01}_{-0.01}$	1.22
S XV	$2.42^{+0.02}_{-0.02}$	1.11
S XVI	$3.03^{+0.07}_{-0.06}$	0.56

Table 6. Properties of the iron line in the spectrum of γ^2 Vel as a function of the orbital phase.

	$\phi = 0.978$	$\phi = 0.078$	$\phi = 0.570$
Line energy (keV)	6.66 ± 0.08	6.67 ± 0.04	6.62 ± 0.03
Equiv. Width (keV)	0.85	0.82	1.18

since the shock front is expected to be wrapped around the O7.5 component.

We found good agreement between the fitting parameters derived for the various SIS and GIS data sets. The results of the simultaneous fits of the SIS and GIS data are listed in Table 3. To allow a comparison with non-solar abundance models, the column densities in Table 3 are given as N_H and $\int \rho \mathrm{d}z$ (in g cm^{-2}, where $\int \rho \mathrm{d}z = 2.38 \times 10^{-24} N_\mathrm{H}$ for a solar-composition material). Our fits yield column densities that are systematically larger than the interstellar value [$N_\mathrm{H}(\mathrm{ISM}) = 8 \times 10^{19}$ cm^{-2}], indicating that most of the absorption must be caused by circumstellar material.

The spectral fits to the *ASCA* data obtained with the 50/50 and 90/10 models and assuming identical compositions for the emitting and absorbing plasmas are described in Table 4. These spectral fits have about the same quality as those obtained assuming solar abundances, except for the $\phi = 0.078$ spectrum. For the $\phi = 0.078$ spectrum, the poorer fit quality results mainly from the fact that the non-solar abundance models fail to reproduce the observed relative intensity of the S XV and XVI lines with respect to the Mg XI and Si XIII lines (see Section 3.2).

The parameters in Table 4 yield systematically higher temperatures (especially for the apastron spectrum) and lower column densities than the solar abundance models. Given the much higher opacities of the WC-wind material, the lower column densities are not unexpected.

3.2 The emission lines

The X-ray spectrum of γ^2 Vel near the phase $\phi = 0.078$ contains several strong emission lines including a rather prominent iron K emission at ~ 6.7 keV (see Fig. 1). We measured the energy and the equivalent width of these lines by fitting a power-law continuum + four Gaussians to the spectrum extracted between 0.7 and 4.0 keV and a power law + Gaussian to the spectrum extracted between 5.0 and 8.0 keV. The results for the four most prominent lines in the 0.7–4.0 keV band measured on the $\phi = 0.078$ spectrum are listed in Table 5. The typical uncertainties on the equivalent width are of the order of 10 per cent for the stronger lines and 15 per cent for the weaker ones. Unfortunately, the limited signal-to-noise ratio of the spectra obtained at an orbital phase $\phi = 0.978$ and 0.570 does not allow us to measure any emission line on these spectra apart from the iron K-shell line.

The Mg, Si and S lines are also detected in the spectrum of the WN5+O6 binary V444 Cyg (Maeda et al. 1999), although with considerably lower equivalent widths and slightly different energies.

Unlike the four lines listed in Table 5, the iron Kα emission at $\sim$6.7 keV is detected in all *ASCA* spectra of γ^2 Vel. Most massive stars have X-ray spectra with temperatures below 1 keV and lack any iron K-shell line near 6.7 keV. The line is, however, seen in the spectra of the colliding wind systems WR 140 (Koyama et al. 1994) and V444 Cyg (Maeda et al. 1999).

The equivalent width of the iron line as a function of orbital phase is listed in Table 6. The strength and energy of this line are rather well reproduced by our best-fitting thermal models. The latter result contrasts with the situation in WR 140, where the power-law shape of the continuum and the strong variability of the iron Kα line point towards a non-thermal phenomenon in the winds of WR 140 (Pollock, Corcoran & Stevens 1999).

4 DISCUSSION AND CONCLUSION

Taking into account the contamination of the X-ray spectrum by the nearby sources, the *ASCA* spectrum of γ^2 Vel mainly consists of a hard thermal emission component that displays strong phase-dependent variability (Fig. 2). The bulk of this variability can be attributed to the changing column density towards the X-ray source, in qualitative agreement with theoretical models of colliding wind binaries (Stevens, Blondin & Pollock 1992; Pittard & Stevens 1997; Walder, Folini & Motamen 1999).

However, the variability also affects the temperature and the luminosity of the hard X-ray emission. In terms of a colliding wind interaction, the difference in temperature of the $\phi = 0.570$ and 0.978 spectrum could be interpreted as a consequence of the wider separation between the two stars at apastron. In fact, the winds are expected to reach higher pre-shock velocities at apastron, while they collide with considerably lower velocities near periastron. [In the strong-shock limit, the post-shock

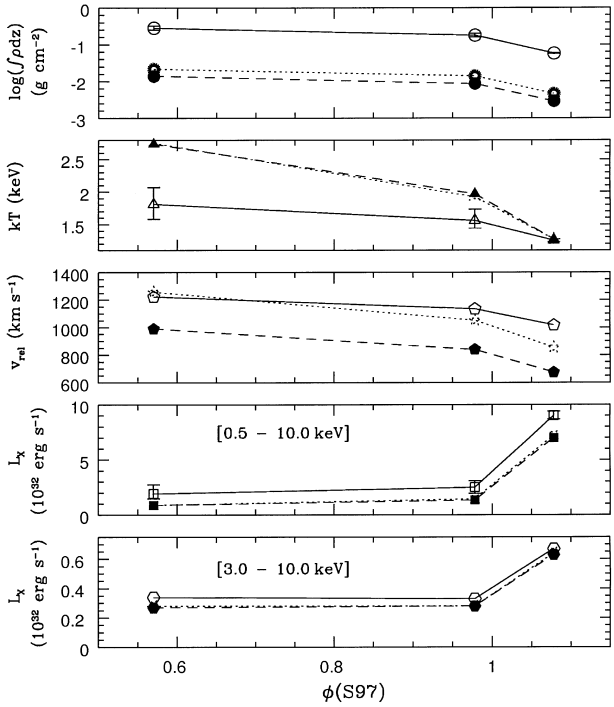

Figure 2. Changes in column density, temperature, relative pre-shock velocity and absorption-corrected luminosity of the hard-emission component in the *ASCA* spectrum of γ^2 Vel as a function of orbital phase (according to the S97 ephemeris). The two lower panels display the intrinsic (absorption-corrected) luminosity in the energy ranges 0.5–10 and 3.0–10 keV. The continuous line indicates the solar composition models, whereas the dotted and dashed lines correspond to the 50/50 and 90/10 non-solar abundance models, respectively. For clarity only the error bars on the parameters of the solar-abundance models have been drawn. The error bars on the luminosities correspond to the 1σ confidence range of the absorbing column density.

temperature is given by the relation $kT = (3/16)\bar{m}v_{\rm rel}^2$ (Stevens et al. 1992), where $\bar{m}$ is the average mass per particle and $v_{\rm rel}$ is the relative pre-shock velocity. In principle, this relationship allows us to derive the relative pre-shock velocities from the temperature of the colliding wind X-ray emission. The values of $v_{\rm rel}$ corresponding to our different models (Tables 3 and 4) are shown in Fig. 2. However, we caution that the actual pre-shock velocity decreases with increasing off-axis angle along the shock front and the temperature of the resulting X-ray emission thus only reflects an average value that certainly underestimates the actual on-axis pre-shock velocity.]

The softest and intrinsically most luminous spectrum is observed at $\phi = 0.078$. A possible explanation could be that the shock region consists of a plasma spanning a rather wide range of temperatures. In this case, a substantial fraction of the softer X-rays may be completely absorbed by the circumstellar material at phases $\phi = 0.978$ and 0.570 and become visible only at a phase $\phi = 0.078$ when the cavity of the O-star wind crosses the line of sight. Alternatively, the lower temperature and higher luminosity at $\phi = 0.078$ could indicate that, at this orbital phase only, the intrinsic emission from the O7.5 III primary star, which we expect to be softer, is significantly contributing to the observed emission. Assuming a bolometric luminosity of the O-star of $2.1 \times 10^5\,{\rm L}_\odot$ (De Marco & Schmutz 1999) and adopting the canonical $L_{\rm X} - L_{\rm bol}$ relation valid for single O-stars (Berghöfer et al. 1997), we find that the intrinsic X-ray emission of the O-star should contribute a

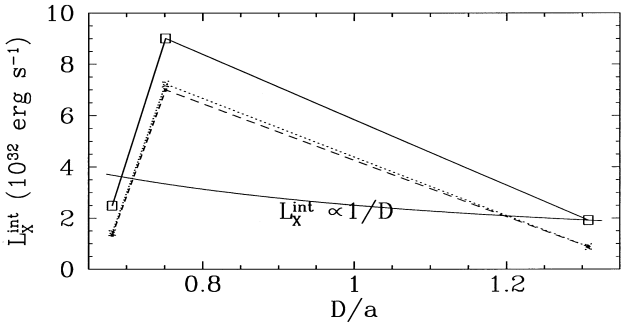

Figure 3. Changes in the absorption-corrected luminosity (0.5–10 keV) of the hard-emission component as a function of orbital separation (according to the S97 ephemeris). The different lines have the same meaning as in Fig. 2. The continuous line labelled $L_{\rm X}^{\rm int} \propto 1/D$ corresponds to the scaling law for adiabatic colliding winds normalized to the luminosity of the solar-abundance apastron model.

luminosity of the order of $1.2 \times 10^{32}\,{\rm erg\,s^{-1}}$. Since Berghöfer et al.'s (1997) relation holds for X-ray luminosities that are not corrected for intrinsic wind absorption, the above estimate should be compared with the $L_{\rm X}$ value at phase $\phi = 0.078$ (Tables 3 and 4). We find that the intrinsic emission from the O-star could indeed account for a significant fraction of the observed X-ray luminosity at a phase of $\phi = 0.078$.

Using the orbital solution of S97 and the scaling law for X-ray emission from largely adiabatic colliding winds, $L_{\rm X} \propto 1/D$, where D is the orbital separation between the stars (Stevens et al. 1992), we would expect a luminosity ratio of 1.7 between the $\phi = 0.078$ and 0.570 spectra and 1.9 between the $\phi = 0.978$ and 0.570 spectra. While the observed ratio between the luminosities at $\phi = 0.078$ and 0.570 is much larger than the 'theoretical' value, whatever the assumed plasma composition, the reverse situation holds for the ratio between the luminosities at $\phi = 0.978$ and 0.570 (see Fig. 3). Fig. 2 also illustrates the variations of the absorption-corrected X-ray flux in the energy band between 3.0 and 10.0 keV which is less affected by the wind absorption and is therefore less sensitive to the uncertainties in the chemical composition of the wind. We find that the disagreement between the measured intrinsic luminosity and the $1/D$ relation persists in the harder energy range. A plausible explanation for the discrepancy between the observed $\phi = 0.978$ versus $\phi = 0.570$ luminosity ratio and the theoretical predictions might be the higher density of the shocked winds near periastron. In fact, as a consequence of the higher density, radiative cooling probably affects the shock properties more efficiently at periastron and hence reduces the hard X-ray emission with respect to the simple scaling law for adiabatic colliding winds. Moreover, the X-ray emission at phase $\phi = 0.978$ could be altered by the shock crushing on to the O-star surface at that orbital phase.

As a result of the large wind momentum ratio between the WR and the O-star wind, St.-Louis et al. (1993) suspected a possible collapse of the shock between the two winds on to the surface of the O-star, at least near periastron. However, Gayley, Owocki & Cranmer (1997) propose that sudden radiative braking might prevent the shock from collapsing on the O-star surface. Using the most recent determination of the wind parameters of the system (Schaerer et al. 1997; De Marco & Schmutz 1999) and the homology relations of Gayley et al. (1997), we find indeed that radiative braking is needed at most orbital phases to prevent a photospheric collision. On the other hand, the temperature and

intrinsic luminosity changes around periastron could also be affected by a time delay between the orbital phase and the occurrence of the expected effects on the wind collision. For instance, the shock could be crushed on to the O-star surface near the periastron passage and might take some time to lift off again.

Corcoran (1996) discussed the variations of the spectral parameters of WR 140 as derived from *ROSAT* PSPC data obtained around periastron passage of this system. We note that in contrast to the γ^2 Vel behaviour displayed in Fig. 2, the temperature of the X-ray spectrum of WR 140 increases strongly around periastron passage.

Considering the position angle of the binary axis with respect to the conjunction at the orbital phases of the *ASCA* observations (Table 1), we notice that the cavity arising from the O-star is probably deflected by the effects of the Coriolis forces (Walder et al. 1999). Willis et al. (1995) suggest a half-opening angle of the shock cone of 25°, while the asymmetry of their *ROSAT* PSPC light curve reflects the effect of the orbital motion. The position angle of the $\phi = 0.078$ *ASCA* observation (Table 1) suggests that the trailing arm of the shock is located at least 32° from the axis of the binary.

We can use the observed column density to the hot component at phase $\phi = 0.570$ when the WC8 star is in front to obtain a rough estimate of the mass-loss rate of this star. Adopting the orbital solution of S97, assuming an orbital inclination of 65° and using the momentum ratio corresponding to the wind parameters of the system (Schaerer et al. 1997; De Marco & Schmutz 1999), we find that the stagnation point (assuming a pure ram-pressure balance) is located at $\sim 32\,R_\odot$ from the centre of the O-star. From this result, we find that the observed column of $\int \rho\,dz = 2.836 \times 10^{-1}\,g\,cm^{-2}$ in the case of the solar-abundance models corresponds to a mass-loss rate of roughly $2 \times 10^{-5}\,M_\odot\,yr^{-1}$. This value is in reasonable agreement with the recent mass-loss determinations by Schaerer et al. (1997) and Stevens et al. (1996). One should, however, notice that this value is strongly dependent on the adopted chemical composition of the absorbing gas and yields probably an *upper limit* on the actual mass-loss rate. Indeed, the non-solar-abundance models yield column densities, and hence mass-loss rates, that are a factor 13 and 20 lower for the 50/50 and 90/10 non-solar-abundance models, respectively.

Maeda et al. (1999) report the analysis of three *ASCA* observations of the short-period (4.2 d) eclipsing binary V444 Cyg (WN5+O6). The fits to these spectra require two-temperature Raymond–Smith models with a soft component at $kT_1 \simeq 0.6$ keV and a harder component at $kT_2 \simeq 2.0$ keV. Maeda et al. find that the column density towards the harder component varies with orbital phase and is largest when the WN5 star is in front. The absorption-corrected luminosity of the hard component in V444 Cyg displays a minimum when the O-star is in front, in agreement with the X-ray source being located between the two stars and rather close to the surface of the O-star. Outside this minimum, the absorption-corrected luminosity (in the 0.7–10 keV energy range and assuming a distance of 1.7 kpc) is of the order of $(1.1\text{–}1.4) \times 10^{33}\,erg\,s^{-1}$, i.e. larger than what is observed for γ^2 Vel.

In contrast to our γ^2 Vel data, the *ASCA* spectra of V444 Cyg reveal no evidence for changes of the temperature of the hard component as a function of orbital phase. In the framework of a colliding wind model, the temperature is indeed expected to remain constant in a binary system with a circular orbit such as V444 Cyg. Let us recall that in the case of the γ^2 Vel data, acceptable fits are achieved with a single-temperature Raymond–Smith model once the contamination by the nearby soft sources is taken into account. In the case of V444 Cyg, there is an additional soft component ($kT_1 \simeq 0.6$ keV) that Maeda et al. (1999) attribute to the intrinsic emission from the WN5 or O6 component. In the case of γ^2 Vel we find no compelling evidence for such a component (except perhaps at phase $\phi = 0.078$).[1] This is not surprising since individual WC stars are on average fainter X-ray sources than individual WN stars (Pollock 1987), and the opaque WC wind material is probably more efficient in absorbing the intrinsic X-ray emission from the O-star in γ^2 Vel.

In summary, our analysis of the three *ASCA* observations of γ^2 Vel reveals a hard-emission component that undergoes strong variability over the orbital cycle. We have constrained the properties of this hard component by accounting for the softer emission from the sources in the vicinity of γ Vel. Our analysis reveals that the uncertainties in the chemical composition of the X-ray emitting plasma significantly affect the derived shock temperature and absorption column, but play a smaller role in determining the intrinsic X-ray luminosity of the colliding wind zone. The observed variations of the hard component are in qualitative agreement with the predictions of colliding wind models, and the column density of the apastron spectrum assuming solar abundances yields an upper limit on the mass-loss rate of the WC8 star of the order of $2 \times 10^{-5}\,M_\odot\,yr^{-1}$ in fair agreement with other recent determinations.

ACKNOWLEDGMENTS

The authors thank an anonymous referee for a careful reading of the manuscript. GR is greatly indebted to the Fonds National de la Recherche Scientifique (Belgium) for support. GR is also supported in part by contract ARC 94/99-178 'Action de recherche concertée de la Communauté Française' (Belgium) and by contract P4/05 'Pôle d'Attraction Interuniversitaire' (SSTC-Belgium). Partial support through the PRODEX XMM-OM Project is also gratefully acknowledged. IRS acknowledges funding from a PPARC Advanced Fellowship. The data reduction was performed on the Starlink node at the University of Birmingham. This research has made use of data obtained from the Leicester Data base and Archive Service at the Department of Physics & Astronomy, Leicester University, UK. The SIMBAD data base has been consulted for the bibliography.

REFERENCES

Abbott D. C., Bieging J. H., Churchwell E., Torres A. V., 1986, ApJ, 303, 239
Abt H. A., Landolt A. U., Levy S. G., Mochnacki S., 1976, AJ, 81, 541
Bałucińska-Church M., McCammon D., 1992, ApJ, 400, 699
Berghöfer T. W., Schmitt J.H.M.M., Cassinelli J. P., 1996, A&AS, 118, 481
Berghöfer T. W., Schmitt J.H.M.M., Danner R., Cassinelli J. P., 1997, A&A, 322, 167
Chapman J. M., Leitherer C., Koribalski B., Bouter R., Storey M., 1999, ApJ, 518, 890
Conti P. S., Smith L. F., 1972, ApJ, 172, 623
Corcoran M. F., 1996, in Niemela V. S., Morrell N., eds, Workshop on Colliding Winds in Binary Stars to honor Jorge Sahade, Rev. Mex. Astron. Astrofis. Ser. Conf., 5, 54
De Marco O., Schmutz W., 1999, A&A, 345, 163
Gayley K. G., Owocki S. P., Cranmer S. R., 1997, ApJ, 475, 786

[1] Willis et al. (1995) fitted the *ROSAT* PSPC data of γ^2 Vel at phases when the O-star is behind the WC8 stellar wind with a blackbody model with $kT \simeq 0.19$ keV. *ASCA* is obviously not the best instrument to detect such a very soft component, especially since the soft energy range is strongly affected by the nearby sources. See also our discussion in Section 3.1.

Hwang U., Mushotzky R. F., Burns J. O., Fukazawa Y., White R. A., 1999, ApJ, 516, 604
Kaastra J. S., 1992, An X-Ray Spectral Code for Optically Thin Plasmas, Internal SRON-Leiden Report
Koyama K., Maeda Y., Tsuru T., Nagase F., Skinner S., 1994, PASJ, 46, L93
Leitherer C., Chapman J. M., Koribalski B., 1997, ApJ, 481, 898
Maeda Y., Koyama K., Yokogawa J., Skinner S., 1999, ApJ, 510, 967
Meynet G., 1999, in van der Hucht K. A., Koenigsberger G., Eenens P. R. J., eds, Wolf–Rayet Phenomena in Massive Stars and Starburst Galaxies, Proc. IAU Symp., Vol. 193. Astron. Soc. Pac., San Francisco, p. 218
Mewe R., Gronenschild E. H. B. M., van den Oord G. H. J., 1985, A&AS, 62, 197
Moffat A. F. J., Vogt N., Paquin G., Lamontagne R., Barrera L. H., 1986, AJ, 91, 1386
Morris P. W., van der Hucht K. A., Willis A. J., Dessart L., Crowther P. A., Williams P. M., 1999, in van der Hucht K. A., Koenigsberger G., Eenens P. R. J., eds, Wolf–Rayet Phenomena in Massive Stars and Starburst Galaxies, Proc. IAU Symp., Vol. 193. Astron. Soc. Pac., San Francisco, p. 77
Pittard J. M., Stevens I. R., 1997, MNRAS, 292, 298
Pollock A. M. T., 1987, ApJ, 320, 283
Pollock A. M. T., Corcoran M. F., Stevens I. R., 1999, in van der Hucht K. A., Koenigsberger G., Eenens P. R. J., eds, Wolf–Rayet Phenomena in Massive Stars and Starburst Galaxies, Proc. IAU Symp., Vol. 193. Astron. Soc. Pac., San Francisco, p. 388
Raymond J. C., Smith B. W., 1977, ApJS, 35, 419
Schaerer D., Schmutz W., Grenon M., 1997, ApJ, 484, L153
Schaller G., Schaerer D., Meynet G., Maeder A., 1992, A&AS, 96, 269
Schmutz W. et al., 1997, A&A, 328, 219 (S97)
St.-Louis N., Willis A. J., Stevens I. R., 1993, ApJ, 415, 298
Stevens I. R., Blondin J. M., Pollock A. M. T., 1992, ApJ, 386, 265
Stevens I. R., Corcoran M. F., Willis A. J., Skinner S. L., Pollock A. M. T., Nagase F., Koyama K., 1996, MNRAS, 283, 589
van der Hucht K. A., Cassinelli J. P., Williams P. M., 1986, A&A, 168, 111
van der Hucht K. A. et al., 1997, New Astron., 2, 245
Walder R., Folini D., Motamen S. M., 1999, in van der Hucht K. A., Koenigsberger G., Eenens P. R. J., eds, Wolf–Rayet Phenomena in Massive Stars and Starburst Galaxies, Proc. IAU Symp., Vol. 193. Astron. Soc. Pac., San Francisco, p. 298
Williams P. M., van der Hucht K. A., Pollock A. M. T., Florkowski D. R., van der Woerd H., Wamsteker W. M., 1990a, MNRAS, 243, 662
Williams P. M., van der Hucht K. A., Sandell G., Thé P. S., 1990b, MNRAS, 244, 101
Willis A. J., Schild H., Stevens I. R., 1995, A&A, 298, 549

This paper has been typeset from a TEX/LATEX file prepared by the author.